



HAL
open science

Fault Trace Corrugation and Segmentation as a Measure of Fault Structural Maturity

I. Manighetti, Antoine Mercier, Louis de Barros

► **To cite this version:**

I. Manighetti, Antoine Mercier, Louis de Barros. Fault Trace Corrugation and Segmentation as a Measure of Fault Structural Maturity. *Geophysical Research Letters*, 2021, 48 (20), pp.e2021GL095372. 10.1029/2021GL095372 . hal-03455176

HAL Id: hal-03455176

<https://hal.science/hal-03455176>

Submitted on 9 Dec 2021

HAL is a multi-disciplinary open access archive for the deposit and dissemination of scientific research documents, whether they are published or not. The documents may come from teaching and research institutions in France or abroad, or from public or private research centers.

L'archive ouverte pluridisciplinaire **HAL**, est destinée au dépôt et à la diffusion de documents scientifiques de niveau recherche, publiés ou non, émanant des établissements d'enseignement et de recherche français ou étrangers, des laboratoires publics ou privés.



Distributed under a Creative Commons Attribution 4.0 International License

Geophysical Research Letters[®]



RESEARCH LETTER

10.1029/2021GL095372

Fault Trace Corrugation and Segmentation as a Measure of Fault Structural Maturity

I. Manighetti¹ , A. Mercier¹ , and L. De Barros¹ 

¹Université Côte d'Azur, Observatoire de la Côte d'Azur, IRD, CNRS, Géoazur, Valbonne, France

Key Points:

- We measure the corrugation and step-over segmentation of 13 large seismogenic fault traces, at scales greater than ~100 m
- The corrugation level and the step-over density, relative width, and size diversity vary with the structural maturity of the faults
- We provide scaling relations measuring fault structural maturity, which should help to describe source faults better in earthquake models

Supporting Information:

Supporting Information may be found in the online version of this article.

Correspondence to:

I. Manighetti,
manighetti@geoazur.unice.fr

Citation:

Manighetti, I., Mercier, A., & De Barros, L. (2021). Fault trace corrugation and segmentation as a measure of fault structural maturity. *Geophysical Research Letters*, 48, e2021GL095372. <https://doi.org/10.1029/2021GL095372>

Received 24 JUL 2021

Accepted 6 OCT 2021

Abstract As faults grow over time and become more “mature,” some of their geometrical and mechanical properties evolve, and these changes modify earthquake behavior. It is thus of prime importance to know the degree of structural maturity of a fault that is likely to produce large earthquakes. Although this concept is extensively used, there is no common definition or metric to measure the structural maturity of a fault. We analyzed the heterogeneity of the surface traces of 13 large seismogenic faults whose maturity is known qualitatively. We measured the corrugations and step-over segmentation of the traces from ~100 m to the fault length scale. Corrugations and some properties of the segmentation are found to vary with fault structural maturity. We provide scaling relationships that quantify the structural maturity of a fault based on its surface trace. These results should help in parameterizing source faults in earthquake models.

Plain Language Summary Long-term faults produce earthquakes. Measuring fault properties could thus help us understand earthquake behavior. However, measuring properties of large-scale faults in particular is difficult. Here, we tackle one of the major long-term properties of faults, their structural maturity. This property relates to the overall slip longevity of the fault (generally several million years), and it has been shown to impact earthquake behavior; mature and immature faults do not behave similarly. For 13 large seismogenic continental faults whose structural maturity was estimated qualitatively in earlier works, we examined the heterogeneity of the traces these faults form at the ground surface. Using simple tools, we measured the undulations and the discrete “stepping” segmentation of the fault traces over a broad range of scales from ~100 m to the full fault length (up to ~1,600 km in this study). We found that the “intensity” of undulations and the density, relative width, and size diversity of the steps separating discrete fault segments all vary with the structural maturity of the faults. These variations are described with simple mathematical functions that characterize fault structural maturity and can be used to better represent source faults in earthquake models.

1. Introduction

Faults are growing features: over geological time, generally, several Myrs, if submitted to tectonic stresses, a fault grows by accumulating slip and lengthening along-strike (e.g., Fossen & Rotevatn, 2016; Manighetti et al., 2001). Generally, the growth occurs through repeated earthquake ruptures. “Structural maturity” is a term coined to describe qualitatively the slip longevity of a fault; the longer the slip history, the more mature the fault. Although the concept appeared in early works (Anderson et al., 1996; Chester et al., 1993; Stirling et al., 1996; Wesnousky, 1988), the term was established more recently (Choy & Kirby, 2004; Manighetti et al., 2007) with attempts of quantification based on classifications of specific fault parameters (initiation age, total cumulative slip, length, and slip rate; Manighetti et al., 2007). Nowadays, the concept of fault structural maturity is extensively used, yet with no common definition nor metrics (e.g., Cheng & Barnhart, 2021; Dascher-Cousineau et al., 2018; DuRoss et al., 2016; Huang, 2018; Kears & Kaneko, 2020; Matera & Bürgmann, 2016; Perrin et al., 2021; Preuss et al., 2019; Thakur et al., 2020).

Fault structural maturity is important because it impacts earthquake behavior. Overall, as a fault becomes more mature, its 3D structure and mechanical properties change, and these changes modify the earthquake properties (e.g., Perrin et al., 2016). In particular, the more mature the fault, the lower the slip to length ratio and hence, possibly, the overall stress drop of the large earthquakes it produces (e.g., Choy & Kirby, 2004; Hecker et al., 2010; Kanamori & Allen, 1986; Manighetti et al., 2007; Radiguet et al., 2009). In this work, we aim to provide metrics to measure the structural maturity of a fault, with a focus on continental seismogenic

© 2021. The Authors.

This is an open access article under the terms of the [Creative Commons Attribution License](https://creativecommons.org/licenses/by/4.0/), which permits use, distribution and reproduction in any medium, provided the original work is properly cited.

faults capable of large earthquakes. Our objective is that these metrics can be used to improve earthquake modeling and hazard assessment.

It is long known that faults are corrugated and segmented laterally at various scales (e.g., Power et al., 1987; Schwartz & Sibson, 1989; Segall & Pollard, 1980; Wesnousky, 1988), and it has been suggested that these geometrical heterogeneities are smoothed out as the fault accumulates more slip (Anderson et al., 1996; Ben-Zion & Sammis, 2003; Brodsky et al., 2011; Choy & Kirby, 2004; Cooke, 1997; Dascher-Cousineau et al., 2018; De Joussineau & Aydin, 2009; Lohr et al., 2008; Nur & Israel, 1980; Perrin et al., 2021; Sagy et al., 2007; Stirling et al., 1996; Wechsler et al., 2010; Wesnousky, 1988). However, measurements supporting these suggestions were generally focused on small scales (corrugations called “roughness”) and local fault sections (Bistacchi et al., 2011; Brodsky et al., 2011, 2015; Brown & Scholz, 1985; Candela et al., 2009, 2012; De Joussineau & Aydin, 2009; Marone & Richardson, 2016; Power et al., 1987; Sagy & Brodsky, 2009), and they were not examined with respect to the structural maturity of the faults.

We approach the question by measuring the >100 m-scale heterogeneity of the surface traces of 13 large (>40 km long) seismogenic normal and strike-slip continental faults worldwide with different levels of structural maturity as qualitatively estimated in earlier works. Using manual maps of the fault traces, we measure the heterogeneity of the traces—namely their corrugation (i.e., undulation) and their lateral segmentation through step-overs, and examine whether this large-scale heterogeneity varies as a function of the supposed structural maturity. We find that both the corrugation level and the step-over size and density vary with the structural maturity of the faults. We produce scaling relations that describe fairly quantitatively the fault structural maturity. These metrics should be useful to input the structural maturity parameter in some earthquake scaling laws (e.g., Manighetti et al., 2007; Radiguet et al., 2009) and to better parameterize large source faults in earthquake models.

2. Data and Method

We selected 13 continental faults whose structural maturity was estimated in earlier works (Perrin et al., 2016) (Table S1 in Supporting Information S1). They span a broad range of lengths (40–1,600 km), initiation ages (2–70 Ma), slip modes (normal and strike-slip), total slips (0.7–400 km), locations worldwide, and tectonic contexts, and thus represent a significant diversity. They include five faults earlier recognized as immature, three as mature, and five as having an “intermediate” maturity. In the latter subset, two faults are fairly mature and one fairly immature (Table S1 in Supporting Information S1).

The surface traces of most of these faults were mapped in earlier works at various resolutions. We had to re-map them to produce a homogeneous mapping from a single source at the same resolution (~ 20 m, Landsat satellite images) (Figure 1; all maps in Figures S1 in Supporting Information S1).

We analyze the main fault trace which accommodates most displacement (e.g., Chester et al., 2004; Sibson, 2003). These traces are generally divided into segments of various lengths, commonly separated by step-overs (Figures 1a, 1d, and S1 in Supporting Information S1). For each fault, we take the shortest of these segments as providing the resolution of the segmentation measures (Table S1 in Supporting Information S1). As most fault traces have a $1\text{--}10^2$ m thickness at the surface (e.g., Sibson, 2003), we consider a conservative uncertainty of 300 m on the across-fault positioning of the traces (Table S1 in Supporting Information S1). The fault maps are vector files where each trace is represented as a series of evenly spaced nodes (Table S1 in Supporting Information S1).

The methods are described in detail in Figures S2 in Supporting Information S1, and the intermediate results are shown for each fault in Figures S3 in Supporting Information S1. First, fault traces are rotated so that the X -axis is the along-fault length. We then analyze the rotated traces in two ways, chosen for their simplicity and lack of a priori on fault curvature, corrugations, segments, and step-overs.

First, we measure the corrugation of the main fault trace, that is, its undulations. For that, we measure the gradient, that is, the angle between the line connecting two consecutive nodes and the X -axis. Defining a sliding window of length L_w , with L_w a variable fraction of the fault length L_f , we calculate the median gradient among the n nodes at a distance $\leq L_w/2$ from the central, sliding node. This allows ignoring the strongest gradients that might result from the fault trace dividing into stepping branches. The window is

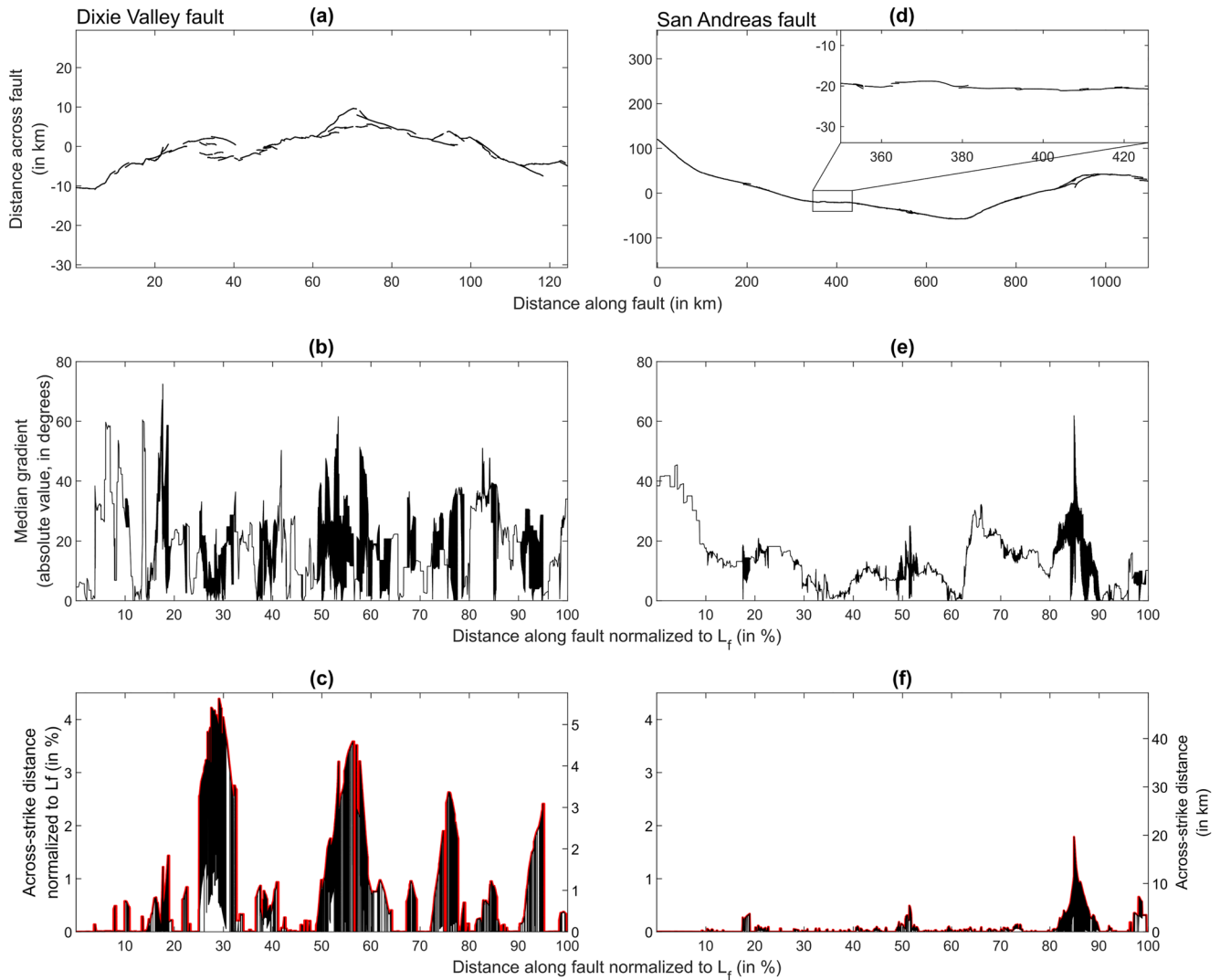


Figure 1. Analysis examples for an immature (Dixie Valley, left) and mature (San Andreas, right) faults. (a) and (d) Main fault traces in the rotated reference frame. Inset in (d) is a close-up on the trace at the same scale as in (a). (b) and (e) Median gradients (absolute values) in sliding window L_w of 2% of fault length L_f . (c) and (f) Across-strike distances among adjacent nodes (black) and derived from a MAX filter among 31 consecutive nodes (red).

made sliding from one node to the next. This provides a dense collection of median gradients along the fault (Figures 1b and 1e), which can be plotted as a histogram. The more corrugated the fault trace is, the wider is the variability in the gradients and the broader is the histogram distribution. To measure the dispersion of the gradients, we fit the gradient histogram with a Gaussian function and use its standard deviation as a proxy for the gradient variability and hence the corrugation level of the fault trace. We perform these measurements with a sliding window of length L_w increasing by 1% steps from 1% to 50% of the total fault length. This allows examining the fault trace corrugations of increasing size, with no a priori of what these corrugations may be. While corrugations captured with small window lengths are primarily undulations in the main fault trace, corrugations detected with longer window lengths also include step-overs.

Second, we measure the step-overs along the fault and hence examine the lateral segmentation of the main fault trace. We measure the across-strike distance between the fault nodes, that is, their separation in the Y-axis direction (Figures 1c and 1f). Step-overs are indeed sites of across-strike distances significantly larger than those between nodes along an undulating trace. To smooth out local meaningless irregularities, we apply a Maximum filter that retains only the largest across-strike distance among a sliding collection of p nodes. We have tested different p values and found that a p subset coinciding with a window length L_w equal

to 2% of the fault length L_f (would the latter be linear and single trace) is a good compromise. Plotting the largest across-strike distance determined in the sliding window as a function of the window position allows locating the step-overs along the fault (Figures 1c and 1f) while measuring their size (along-strike length and across-fault width) and counting their number.

3. Results

The standard deviation of the median gradient distribution is shown for all faults as a function of the sliding window length L_w in Figure 2a (additional measures in Figures S4 in Supporting Information S1, Figures A–D). The functions are tightly grouped and similar beyond L_w of 25%–30% L_f . This shows that none of the faults have significant corrugations longer than 25%–30% of the fault length. By contrast, for shorter L_w , the functions are markedly different, showing a gradation from fairly flat curve sections with low standard deviation (around 5) at the smallest L_w , to increasingly steeping curve sections with standard deviations from ~ 10 to 25 at the smallest L_w . The gradation seems coincident with the increasing structural maturity of the faults (Table S1 in Supporting Information S1): the most mature faults show flat, low standard deviation functions; conversely, the most immature faults have the largest standard deviation functions, with the steepest decrease.

The shape of the curves in Figure 2a provides information on the fault trace heterogeneity. A fairly flat section indicates that the fault trace has no or little corrugations at length scales of about the window length at which the curve flattens. Conversely, a pronounced slope in the curve indicates the presence of significant corrugations of lengths in the L_w range of the slope. These most prominent corrugation scales are best revealed through the variations of the standard deviation of the median gradient distribution (Figure 2b). The most mature faults have a single significant length scale of corrugations, less than $\sim 5\%$ of the fault length; whereas the most immature faults show different lengths of corrugations, up to 25%–30% of L_f .

Figure 2c shows the number of step-overs per kilometer of fault length (which we later referred to as step-over density), as a function of their relative width (see also Figures S4 in Supporting Information S1, Figure E). For all step-over sizes, the density of step-overs differs by the structural maturity of the fault: immature faults have systematically the largest step-over densities, and mature faults have the lowest. The largest relative size of the step-overs also varies with the structural maturity of the fault, with the largest step-overs (relative size) on immature faults, and the smallest ones (relative size) on mature faults. However, when step-over absolute sizes are examined, an opposite relation is found (Figures S4 in Supporting Information S1, Figure Fa). Whatever the structural maturity of a fault, the step-over density decreases with increasing relative step-over size. For each fault in Figure 2c, we calculate the median step-over relative width associated with each density value. We then estimate the power law that best fits these measures. Figure 2d shows that not only the step-over density varies with the structural maturity of the faults, but also does the density decay rate as a function of the step-over relative width: the decay is “faster” for immature faults and “slower” for mature faults. As the largest relative widths of step-overs are in a narrow range (2%–9% L_f) for all faults (Figure 2d), the differences in decay rate are primarily controlled by differences in step-over densities among faults; mature faults share fairly constant, low step-over densities, whereas immature faults have higher yet markedly variable step-over densities.

The length and the total displacement on a fault are commonly taken as proxies of its structural maturity (e.g., Perrin et al., 2021 and references therein). Figures 3a and 3b show the standard deviation of the median gradient distribution (at L_w of 2% L_f , thus small scale) as a function of fault length and total displacement, respectively (other L_w in Figures S4 in Supporting Information S1, Figures G–H). A power law function fits the data reasonably well, suggesting that a relation exists between the fault length or the total displacement and the small-scale corrugation level of the fault trace. Figures 3c and 3d show the density of step-overs wider than 0.1% L_f as a function of fault length and total displacement, respectively (other step-over widths in Figures S4 in Supporting Information S1, Figure I). As step-overs are examined here down to very small scales (minimum width of 0.1% L_f), the total numbers of step-overs used to build Figures 3c and 3d well represent the total numbers of step-overs along the faults. In both Figures 3c and 3d, a power law function fits the data fairly well, suggesting a relation between step-over density and both fault length and total displacement. However, as the slope is about -1 in Figure 3c, the relation may be primarily controlled by the fault

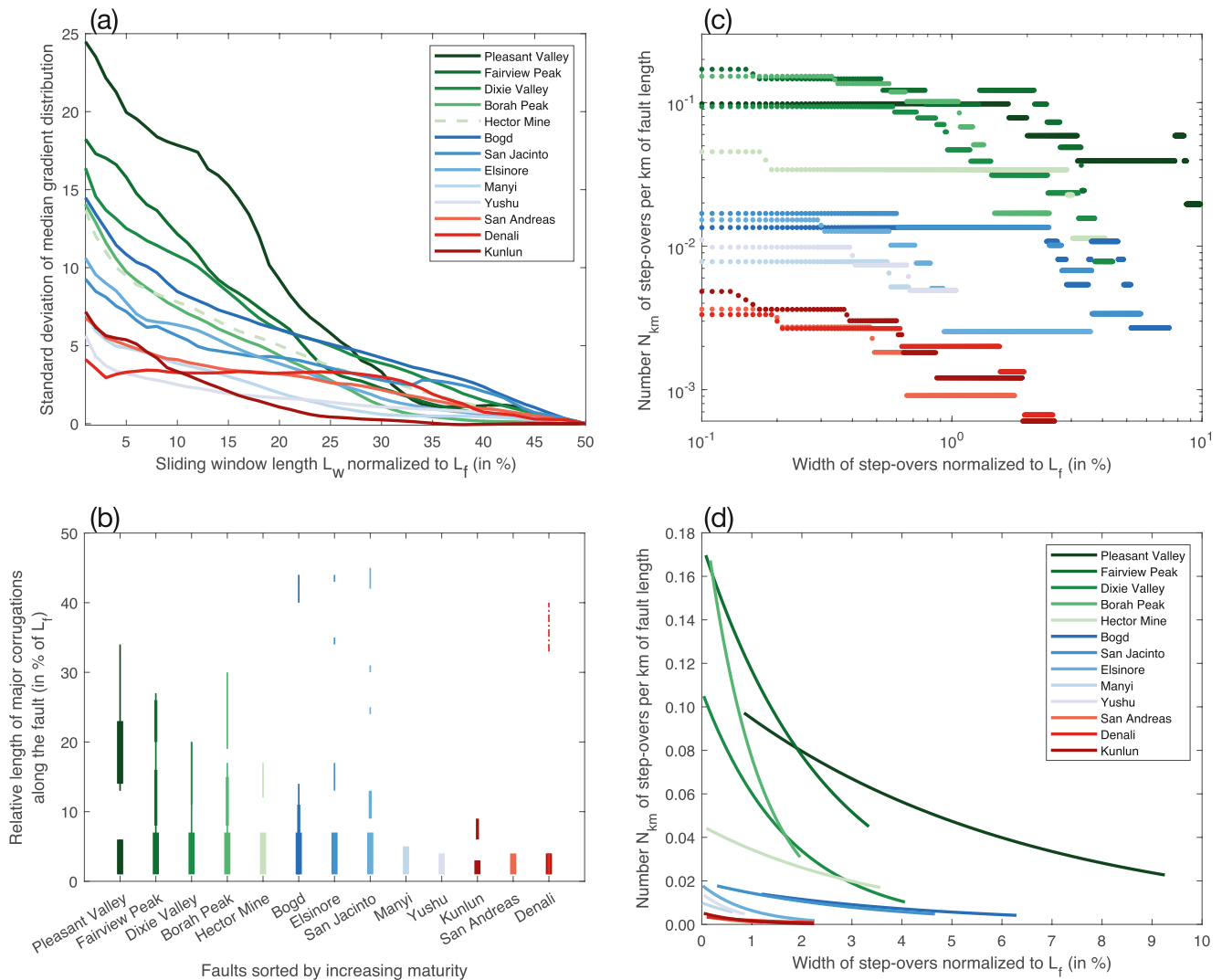


Figure 2. Corrugation and step-over segmentation of main fault traces. In all graphs, colors indicate *a priori* knowledge of fault structural maturity (Table S1 in Supporting Information S1), with red, blue, and green tones for mature, “intermediate,” and immature faults, respectively. Some faults are named as their most recent large earthquake. (a) Corrugation measured with standard deviation (Sd) of median gradient distribution, as a function of sliding window length L_w normalized to L_f . All curves are corrected from the overall curvature of the fault trace by setting Sd to 0 at L_w of $50\%L_f$ (see Figures S2–S4 in Supporting Information S1). Hector Mine is dotted because Sd is poorly constrained at small L_w . (b) Dominant corrugation length scales along faults. The graph shows the peaks higher than 0.25 in the variations of the standard deviation of the median gradient distribution (Figures S3 in Supporting Information S1, Figure 9). Line thickness increases with the height of the peaks, thus with the most prominent corrugation length scales. Dotted for Denali is a peak resulting from the overall fault curvature. (c) Number of step-overs per km of fault length as a function of their across-fault width. The graph shows the number of step-overs having a width larger than a threshold size, which varies along X by 0.01 steps (in % L_f). Original measures in Figures S3 in Supporting Information S1, Figure 13c. Here, these original values have been smoothed with a Median filter on a 100-sample sliding window (other filters in Figures S4 in Supporting Information S1, Figure E). (d) Best power-law fit of functions in (c). For each fault, to each plateau at constant density Y_c in Figure 2c, we assign the median step-over width W_{med} (see Figures S2 in Supporting Information S1). We then calculate the power law function that best-fits the Y_c – W_{med} points.

length. The inset graphs in Figures 3c and 3d confirm that the total number of step-overs wider than $0.1\% L_f$ is fairly similar among faults regardless of their structural maturity, with most faults having 6–12 step-overs. As the total number of step-overs, the length-to-width ratio of the step-overs, of ~ 4 , is fairly similar among faults regardless of their maturity (Figures S4 in Supporting Information S1, Figure J).

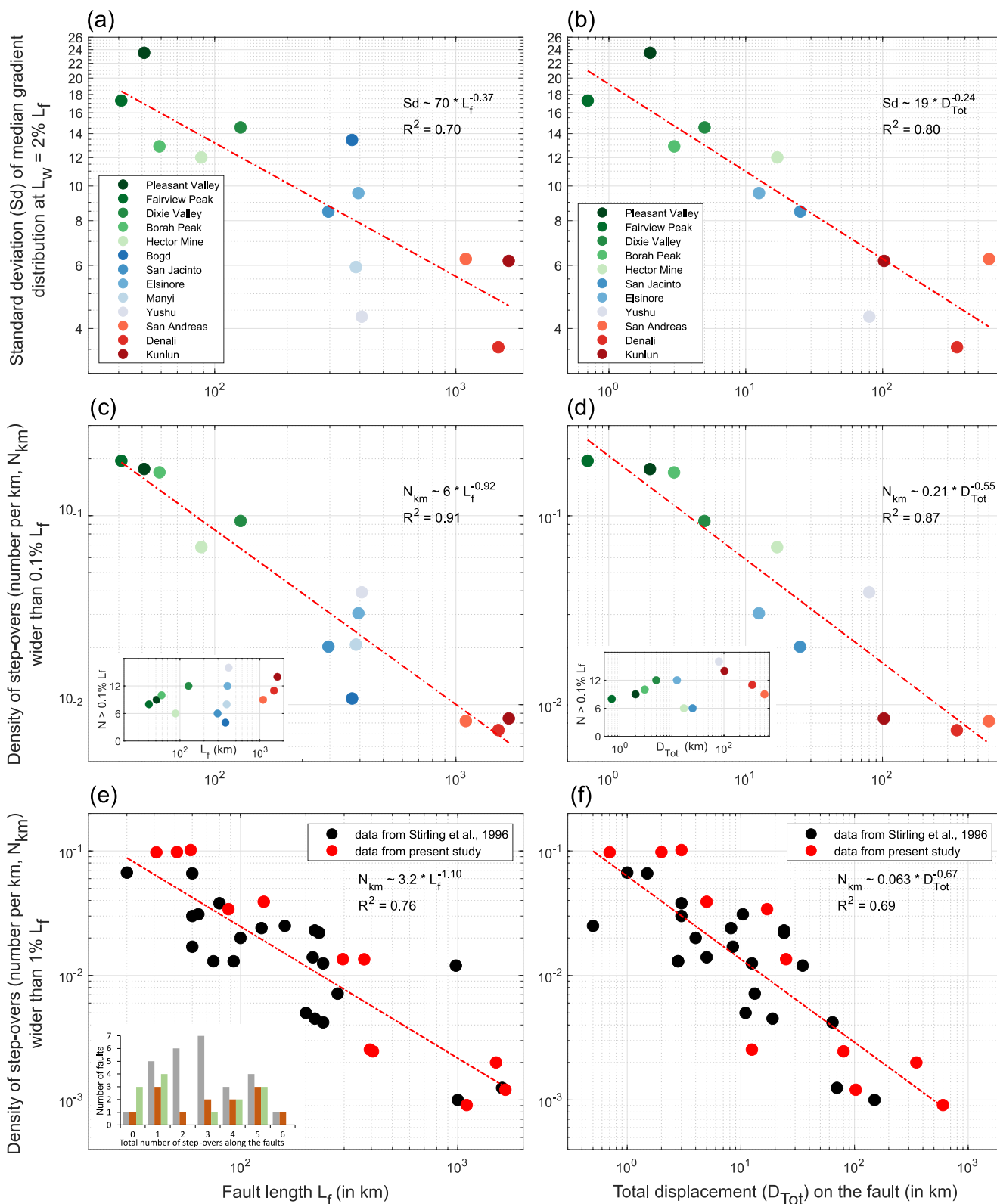


Figure 3.

4. Discussion and Conclusions

Our results confirm that surface fault traces are significantly undulated and segmented at various scales, here greater than ~ 100 m. We additionally show that these corrugation and segmentation vary with the structural maturity of the faults, independently of the type of faulting (strike-slip and normal faults analyzed here). Furthermore, the scaling relations that we find demonstrate that fault traces at the ground surface record and preserve fundamental features of the fault and earthquake processes that occur at greater depth.

Figure 2a demonstrates that, as a fault becomes more mature, the corrugation level of its surface trace decreases; that is, the fault trace becomes smoother. This has been suggested in earlier works, mainly based on measurements at small outcrop scales (references in Section 1), but never shown at such a large scale on major seismogenic faults that furthermore span a large diversity. Additionally, the smoothing of the smallest corrugations is at least partly deterministic: a simple relation describes it fairly well, as a function of both fault length and total displacement (Figures 3a and 3b).

The relation between fault lateral segmentation and structural maturity is more complex. Several features of the fault segmentation seem to be independent of fault maturity. While the total number of step-overs varies with the size range examined (Figures S4 in Supporting Information S1, Figure F), for every size range the total number of step-overs, and hence of fault segments, is fairly similar among faults regardless of their maturity (insets, Figures 3c and 3d). When largest step-overs are considered, their number is few and similar among faults, ≤ 6 and more generally ≤ 3 , indicating that, regardless of their maturity, faults are divided into a similar, limited number of major segments, generally 2–4 (inset, Figure 3e). This is in keeping with earlier findings that showed that the number of largest segments along faults is generic, ~ 2 –4 (De Joussineau & Aydin, 2009; Otsuki & Dilov, 2005; Manighetti et al., 2009, 2015). The length to width ratio of the step-overs also seems to be fairly constant (~ 4), as suggested in earlier works (e.g., Aydin & Nur, 1982; De Joussineau & Aydin, 2009; Long & Imber, 2011; Fossen & Rotevatn, 2016), and thus independent of the fault structural maturity. Consequently, as more mature faults tend to be longer, the step-over density along a fault decreases with its structural maturity (Figures 3c and 3d), as does the largest relative width of the step-overs (Figure 2c) and the variability of the step-over sizes along the fault (Figures 2b and 2d).

To discuss these observations, we come back to the original definition of structural maturity, that is, the slip longevity of a fault. Immature faults are those with a short slip history ($< a$ few Ma, Manighetti et al., 2007), and as such, they provide information on the early stages of fault growth. Our findings suggest that, in these early stages, a fault is relatively short and its surface trace is both highly corrugated and showing a great density (number of step-overs per kilometer of fault) of segments of various lengths from < 1 to 25%–30% L_f (Figure 2b). The largest step-overs are wide, up to 10% L_f (Figure 2c). In contrast, mature faults, which represent much later stages of fault growth, are longer and have a smooth trace in between the step-overs. While they have about the same number of step-overs as immature faults (insets, Figures 3c and 3d), due to their longer length their step-overs are much less dense and have much smaller relative width than on immature faults. However, as the length to width ratio of step-overs is fairly constant, step-overs on mature faults can have large absolute widths, up to 40 km on Kunlun and Denali (see also Figure 1f).

That fault traces are highly corrugated in the early stages of fault growth implies that faults are originally made of very short sections with different strikes, all in all forming an undulating trace. This is consistent with the observation of faulted laboratory rock samples (e.g., Moore & Lockner, 1995) and confirming that faults grow and propagate out-of-plane (Cooke & Madden, 2014; Fossen & Rotevatn, 2016; Jackson, 1987; Preuss et al., 2019).

Figure 3. Corrugation level and step-over density as a function of fault length and total displacement (at sliding window $L_w = 2\%L_f$). In all graphs, fault lengths and displacements from Table S1 in Supporting Information S1; red curve is the best-fitting regression with power law. In (a)–(d) colors show *a priori* knowledge of fault structural maturity, as in Figure 2. (a)–(b) Standard deviation (Sd) of median gradient distribution (from Figure 2a) as a function of fault length L_f and total displacement D_{Tot} , respectively. (c)–(d) Density of step-overs wider than 0.1% of L_f (from Figures S3 in Supporting Information S1, Figure 13), as a function of fault length L_f and total displacement D_{Tot} , respectively. Insets present the total number N of step-overs wider than 0.1% L_f as a function of L_f or D_{Tot} . (e)–(f) Density of step-overs wider than 1% of L_f as a function of fault length L_f and total displacement D_{Tot} , respectively. Red and black, data from this study and from Stirling et al. (1996), respectively. Inset shows the distribution of the total number of largest step-overs along the faults. In brown and green, step-overs in our data that are wider than 1% and 2% L_f , respectively. In gray, data from Stirling et al. (1996). While the threshold size of step-overs is not indicated in Stirling et al. (1996), they are the largest along the faults, mapped at low resolution.

As a fault matures, the corrugations of its trace are smoothed out, making the fault more continuous and straighter. How this happens is unclear but the fracturing of step-over zones allowing fault segments to coalesce and abrasional wear have been proposed as likely mechanisms (e.g., Brodsky et al., 2011; Dascher-Cousineau et al., 2018; Fossen & Rotevatn, 2016; Lee & Bruhn, 1996; Power et al., 1987, 1988; Sagy et al., 2007). The smoothing of the smallest corrugations observed here seems to be partly deterministic, increasing with fault slip (Figure 3b).

That the number of step-overs, but also their length to width ratio, are similar among faults with different maturity and among step-overs of different sizes, suggests that step-overs are a generic and deterministic output of the fault mechanics. Over the long-term, faults grow through alternating phases of slip accumulation at fairly constant length-producing increasing stress and damage at fault tips, and of along-strike lengthening-through prior damage (Bull et al., 2006; Giba et al., 2012; Nicol et al., 2005; Schlagenhauf et al., 2008). Such a bimodal growth may explain the generic segmentation as it may progressively create new step-overs ahead of the growing fault with a size increasing with stress at fault tips and hence with fault length (Aydin & Berryman, 2010; Manighetti et al., 2009, 2015; Schlagenhauf et al., 2008). That the total number of step-overs is constant along faults suggests however that, as new step-overs are created, some of the pre-existing ones, likely the smallest step-overs, are smoothed out (De Jousineau & Aydin, 2009; Fossen & Rotevatn, 2016; Lohr et al., 2008; Sagy et al., 2007; Stirling et al., 1996; Wesnousky, 1988). This smoothing likely leaves a corrugated, yet more continuous fault trace.

Thus, while faults are divided into a similar number of major segments whatever their maturity (insets in Figure 3), these segments become longer (bimodal fault growth), more planar (less corrugations, Figures 2a, 2b, 3a and 3b), and smoother (punctuated with less dense and relatively smaller step-overs, Figures 2c, 2d, 3c and 3d) as the fault becomes more mature. Major segments along mature faults thus form longer asperities with more homogeneous strength and lower fracture energy than those on immature faults. This makes mature faults more prone to produce long earthquake ruptures propagating easily and at fast speed on the fault plane and having fairly low stress drop (e.g., Manighetti et al., 2007; Perrin et al., 2016, 2021). Conversely, immature faults are expected to produce shorter, slower, yet more energetic ruptures (Böse & Heaton, 2010; Choy & Kirby, 2004; Fang & Dunham, 2013; Manighetti et al., 2007; Newman & Griffith, 2014; Perrin et al., 2016; Radiguet et al., 2009; Sagy et al., 2007).

We show here that the corrugation level and the step-over density of a surface fault trace are two relevant metrics to quantify the structural maturity of the fault. The measurements were done at a fairly low resolution, demonstrating that there is no need to map a fault at a high resolution to derive the metrics properly. Furthermore, as the corrugation level and step-over density can be expressed in units of fault length, there is no need either to map a fault trace entirely: as faults do not seem to have corrugations and hence segments longer than 25%–30% of their length (Figures 2a and 2b), analyzing a third of a fault trace should be sufficient to derive the metrics, provided that this section encloses the most mature part of the fault (demonstration in Figures S4 in Supporting Information S1, Figure K). However, while these should reduce the time of analysis, mapping a third a long fault may still be time consuming.

In a fault trace map, the standard deviation of the median gradient distribution can be measured. For the smallest window lengths, it is expected to be 5 ± 1 for a mature fault, 10 ± 1 for a fault with intermediate maturity, and 14–25 for an immature fault (Figure 2a). Meanwhile, the step-over density (as in Figure 2c) is expected to be $\sim 10^{-3}$ for a mature fault, $\sim 10^{-2}$ for a fault with intermediate maturity, and $\sim 10^{-1}$ for an immature fault (Figure 2c). The scaling relations of Figure 3 can also be used to derive the maturity of a fault. As it is easier to identify and measure step-overs than corrugations, especially the largest step-overs, we suggest that the scaling relations in Figures 3e and 3f may be more practical (see also Figures S4 in Supporting Information S1, Figure L). They combine our measurements of the largest step-overs and those of Stirling et al. (1996) that also concern the largest step-overs identified in low-resolution, published maps. Although the structural maturity is not informed in the figures, data falling in the upper left and lower right parts of the graphs represent immature and mature faults, respectively.

Nowadays, deep learning can efficiently assist geologists to map surface fault traces automatically at high resolution and accuracy in optical images of the ground (Mattéo et al., 2021). This provides the opportunity to rapidly map the surface traces of many faults worldwide, and to analyze them as described here to recover

the structural maturity of these faults. As fault structural maturity impacts earthquake behavior (references in Introduction), its knowledge should improve earthquake hazard assessment. One way may be to input the maturity knowledge into the few available empirical relations that link fault maturity and earthquake slip or ground motions (Manighetti et al., 2007; Radiguet et al., 2009), and derive the expected largest earthquake magnitudes. Another way may be to use the functions in Figures 2 and 3 to parameterize the model of a fault so as to provide realistic dynamic rupture scenarios prior to its rupture. The a priori knowledge of the structural maturity of a fault being ruptured may also improve Earthquake Early Warning, as recently suggested by Böse et al. (2021) and Hutchison et al. (2020).

Data Availability Statement

Fault trace data are provided as QGIS shapefiles on a repository at <https://doi.org/10.5281/zenodo.5411798>. All other information is provided as Supplementary documents (Table S1 and Figures S1–S4 in Supporting Information S1).

Acknowledgments

This work has been done in the framework of the ANR project FAULTS_R_GEMS (ANR-17-CE31-0008). The authors thank Clément Perrin for his contribution to preliminary versions of the fault maps and for great discussions. The authors also thank Editor German Prieto and two anonymous reviewers for their thorough comments that helped them to improve the manuscript.

References

- Anderson, J. G., Wesnousky, S. G., & Stirling, M. W. (1996). Earthquake size as a function of fault slip rate. *Bulletin of the Seismological Society of America*, 86(3), 683–690.
- Aydin, A., & Berryman, J. G. (2010). Analysis of the growth of strike-slip faults using effective medium theory. *Journal of Structural Geology*, 32(11), 1629–1642. <https://doi.org/10.1016/j.jsg.2009.11.007>
- Aydin, A., & Nur, A. (1982). Evolution of pull-apart basins and their scale independence. *Tectonics*, 1(1), 91–105. <https://doi.org/10.1029/TC001i001p00091>
- Ben-Zion, Y., & Sammis, C. G. (2003). Characterization of fault zones. *Pure and Applied Geophysics*, 160(3), 677–715. <https://doi.org/10.1007/PL00012554>
- Bistacchi, A., Griffith, W. A., Smith, S. A., Di Toro, G., Jones, R., & Nielsen, S. (2011). Fault roughness at seismogenic depths from LIDAR and photogrammetric analysis. *Pure and Applied Geophysics*, 168(12), 2345–2363. <https://doi.org/10.1007/s00024-011-0301-7>
- Böse, M., & Heaton, T. H. (2010). Probabilistic prediction of rupture length, slip and seismic ground motions for an ongoing rupture: Implications for early warning for large earthquakes. *Geophysical Journal International*, 183(2), 1014–1030. <https://doi.org/10.1111/j.1365-246X.2010.04774.x>
- Böse, M., Hutchison, A., Manighetti, I., Li, J., Massin, F., & Clinton, J. (2021). FinDerS(+) - real-time slip profiles and magnitudes estimated from backprojected seismic and geodetic displacement amplitudes. *Frontiers of Earth Science*, 9. <https://doi.org/10.3389/feart.2021.685879>
- Brodsky, E. E., Gilchrist, J. J., Sagy, A., & Collettini, C. (2011). Faults smooth gradually as a function of slip. *Earth and Planetary Science Letters*, 302(1–2), 185–193. <https://doi.org/10.1016/j.epsl.2010.12.010>
- Brown, S. R., & Scholz, C. H. (1985). Broad bandwidth study of the topography of natural rock surfaces. *Journal of Geophysical Research*, 90(B14), 12575–12582. <https://doi.org/10.1029/JB090iB14p12575>
- Bull, J. M., Barnes, P. M., Lamarche, G., Sanderson, D. J., Cowie, P. A., Taylor, S. K., & Dix, J. K. (2006). High-resolution record of displacement accumulation on an active normal fault: Implications for models of slip accumulation during repeated earthquakes. *Journal of Structural Geology*, 28(7), 1146–1166. <https://doi.org/10.1016/j.jsg.2006.03.006>
- Candela, T., Renard, F., Bouchon, M., Brouste, A., Marsan, D., Schmittbuhl, J., & Voisin, C. (2009). Characterization of fault roughness at various scales: Implications of three-dimensional high resolution topography measurements mechanics, structure and evolution of fault zones. *Birkhäuser Basel*, 1817–1851. https://doi.org/10.1007/978-3-0346-0138-2_13
- Candela, T., Renard, F., Klinger, Y., Mair, K., Schmittbuhl, J., & Brodsky, E. E. (2012). Roughness of fault surfaces over nine decades of length scales. *Journal of Geophysical Research: Solid Earth*, 117(B8), B08409. <https://doi.org/10.1029/2011JB009041>
- Cheng, G., & Barnhart, W. D. (2021). Permanent co-seismic deformation of the 2013 Mw7.7 Baluchistan, Pakistan earthquake from high-resolution surface strain analysis. *Journal of Geophysical Research: Solid Earth*, 126(3), e2020JB020622. <https://doi.org/10.1029/2020JB020622>
- Chester, F. M., Chester, J. S., Kirschner, D. L., Schulz, S. E., & Evans, J. P. (2004). Structure of large-displacement, strike-slip fault zones in the brittle continental crust. In *Rheology and Deformation of the Lithosphere at continental Margins* (pp. 223–260). Columbia University Press. <https://doi.org/10.7312/karn12738-009>
- Chester, F. M., Evans, J. P., & Biegel, R. L. (1993). Internal structure and weakening mechanisms of the San Andreas fault. *Journal of Geophysical Research*, 98(B1), 771–786. <https://doi.org/10.1029/92jb01866>
- Choy, G. L., & Kirby, S. H. (2004). Apparent stress, fault maturity and seismic hazard for normal-fault earthquakes at subduction zones. *Geophysical Journal International*, 159(3), 991–1012. <https://doi.org/10.1111/j.1365-246X.2004.02449.x>
- Cooke, M. L. (1997). Fracture localization along faults with spatially varying friction. *Journal of Geophysical Research*, 102(B10), 22425–22434. <https://doi.org/10.1029/97jb01829>
- Cooke, M. L., & Madden, E. H. (2014). Is the Earth lazy? A review of work minimization in fault evolution. *Journal of Structural Geology*, 66, 334–346. <https://doi.org/10.1016/j.jsg.2014.05.004>
- Dascher-Cousineau, K., Kirkpatrick, J. D., & Cooke, M. L. (2018). Smoothing of fault slip surfaces by scale-invariant wear. *Journal of Geophysical Research: Solid Earth*, 123(9), 7913–7930.
- De Joussineau, G., & Aydin, A. (2009). Segmentation along strike-slip faults revisited. *Pure and Applied Geophysics*, 166(10), 1575–1594. <https://doi.org/10.1007/s00024-009-0511-4>
- DuRoss, C. B., Personius, S. F., Crone, A. J., Olig, S. S., Hylland, M. D., Lund, W. R., & Schwartz, D. P. (2016). Fault segmentation: New concepts from the Wasatch fault zone, Utah, USA. *Journal of Geophysical Research: Solid Earth*, 121(2), 1131–1157. <https://doi.org/10.1002/2015JB012519>

- Fang, Z., & Dunham, E. M. (2013). Additional shear resistance from fault roughness and stress levels on geometrically complex faults. *Journal of Geophysical Research: Solid Earth*, 118(7), 3642–3654. <https://doi.org/10.1002/jgrb.50262>
- Fossen, H., & Rotevatn, A. (2016). Fault linkage and relay structures in extensional settings—A review. *Earth-Science Reviews*, 154, 14–28. <https://doi.org/10.1016/j.earscirev.2015.11.014>
- Giba, M., Walsh, J. J., & Nicol, A. (2012). Segmentation and growth of an obliquely reactivated normal fault. *Journal of Structural Geology*, 39, 253–267. <https://doi.org/10.1016/j.jsg.2012.01.004>
- Hecker, S., Dawson, T. E., & Schwartz, D. P. (2010). Normal-faulting slip maxima and stress-drop variability: A geological perspective. *Bulletin of the Seismological Society of America*, 100(6), 3130–3147. <https://doi.org/10.1785/0120090356>
- Huang, Y. (2018). Earthquake rupture in fault zones with along-strike material heterogeneity. *Journal of Geophysical Research: Solid Earth*, 123(11), 9884–9898. <https://doi.org/10.1029/2018JB016354>
- Hutchison, A. A., Böse, M., & Manighetti, I. (2020). Improving early estimates of large earthquake's final fault lengths and magnitudes leveraging source fault structural maturity information. *Geophysical Research Letters*, 47(14), e2020GL087539. <https://doi.org/10.1029/2020GL087539>
- Jackson, P. (1987). The corrugation and bifurcation of fault surfaces by cross-slip. *Journal of Structural Geology*, 9(2), 247–250. [https://doi.org/10.1016/0191-8141\(87\)90030-7](https://doi.org/10.1016/0191-8141(87)90030-7)
- Kanamori, H., & Allen, C. R. (1986). *Earthquake Source Mechanics* Geophysical Monograph (Vol. 37, pp. 227–235). American Geophysical Union.
- Kearse, J., & Kaneko, Y. (2020). On-fault geological fingerprint of earthquake rupture direction. *Journal of Geophysical Research: Solid Earth*, 125(9), e2020JB019863. <https://doi.org/10.1029/2020JB019863>
- Lee, J. J., & Bruhn, R. L. (1996). Structural anisotropy of normal fault surfaces. *Journal of Structural Geology*, 18(8), 1043–1059. [https://doi.org/10.1016/0191-8141\(96\)00022-3](https://doi.org/10.1016/0191-8141(96)00022-3)
- Lohr, T., Krawczyk, C. M., Oncken, O., & Tanner, D. C. (2008). Evolution of a fault surface from 3D attribute analysis and displacement measurements. *Journal of Structural Geology*, 30(6), 690–700. <https://doi.org/10.1016/j.jsg.2008.02.009>
- Long, J. J., & Imber, J. (2011). Geological controls on fault relay zone scaling. *Journal of Structural Geology*, 33(12), 1790–1800. <https://doi.org/10.1016/j.jsg.2011.09.011>
- Manighetti, I., Campillo, M., Bouley, S., & Cotton, F. (2007). Earthquake scaling, fault segmentation, and structural maturity. *Earth and Planetary Science Letters*, 253(3–4), 429–438. <https://doi.org/10.1016/j.epsl.2006.11.004>
- Manighetti, I., Caulet, C., De Barros, L., Perrin, C., Cappa, F., & Gaudemer, Y. (2015). Generic along-strike segmentation of A far normal faults, East Africa: Implications on fault growth and stress heterogeneity on seismogenic fault planes. *Geochemistry, Geophysics, Geosystems*, 16(2), 443–467. <https://doi.org/10.1002/2014GC005691>
- Manighetti, I., King, G. C. P., Gaudemer, Y., Scholz, C. H., & Doubre, C. (2001). Slip accumulation and lateral propagation of active normal faults in Afar. *Journal of Geophysical Research: Solid Earth*, 106(B7), 13667–13696. <https://doi.org/10.1029/2000JB900471>
- Manighetti, I., Zigone, D., Campillo, M., & Cotton, F. (2009). Self-similarity of the largest-scale segmentation of the faults: Implications for earthquake behavior. *Earth and Planetary Science Letters*, 288(3–4), 370–381. <https://doi.org/10.1785/0120080340>
- Marone, C., & Richardson, E. (2016). Research focus: Connections between fault roughness, dynamic weakening, and fault zone structure. *Geology*, 44(1), 79–80. <https://doi.org/10.1130/focus012016.1>
- Materna, K., & Bürgmann, R. (2016). Contrasts in compliant fault zone properties inferred from geodetic measurements in the San Francisco Bay area. *Journal of Geophysical Research: Solid Earth*, 121(9), 6916–6931. <https://doi.org/10.1002/2016JB013243>
- Mattéo, L., Manighetti, I., Tarabalka, Y., Gaucel, J. M., Van Den Ende, M., Mercier, A., et al. (2021). Automatic fault mapping in remote optical images and topographic data with deep learning. *Journal of Geophysical Research: Solid Earth*, 126, e2020JB021269. <https://doi.org/10.1029/2020JB021269>
- Moore, D. E., & Lockner, D. A. (1995). The role of microcracking in shear-fracture propagation in granite. *Journal of Structural Geology*, 17(1), 95–114. [https://doi.org/10.1016/0191-8141\(94\)E0018-T](https://doi.org/10.1016/0191-8141(94)E0018-T)
- Newman, P. J., & Griffith, W. A. (2014). The work budget of rough faults. *Tectonophysics*, 636, 100–110. <https://doi.org/10.1016/j.tecto.2014.08.007>
- Nicol, A., Walsh, J., Berryman, K., & Nodder, S. (2005). Growth of a normal fault by the accumulation of slip over millions of years. *Journal of Structural Geology*, 27(2), 327–342. <https://doi.org/10.1016/j.jsg.2004.09.002>
- Nur, A., & Israel, M. (1980). The role of heterogeneities in faulting. *Physics of the Earth and Planetary Interiors*, 21(2–3), 225–236. [https://doi.org/10.1016/0031-9201\(80\)90072-2](https://doi.org/10.1016/0031-9201(80)90072-2)
- Otsuki, K., & Dilov, T. (2005). Evolution of hierarchical self-similar geometry of experimental fault zones: Implications for seismic nucleation and earthquake size. *Journal of Geophysical Research: Solid Earth*, 110(B3), B03303. <https://doi.org/10.1029/2004JB003359>
- Perrin, C., Manighetti, I., Ampuero, J. P., Cappa, F., & Gaudemer, Y. (2016). Location of largest earthquake slip and fast rupture controlled by along-strike change in fault structural maturity due to fault growth. *Journal of Geophysical Research: Solid Earth*, 121(5), 3666–3685. <https://doi.org/10.1002/2015JB012671>
- Perrin, C., Waldhauser, F., & Scholz, C. H. (2021). The shear deformation zone and the smoothing of faults with displacement. *Journal of Geophysical Research: Solid Earth*, 126(5), e2020JB020447. <https://doi.org/10.1029/2020JB020447>
- Power, W. L., Tullis, T. E., Brown, S. R., Boitnott, G. N., & Scholz, C. H. (1987). Roughness of natural fault surfaces. *Geophysical Research Letters*, 14(1), 29–32. <https://doi.org/10.1029/GL014i001p00029>
- Power, W. L., Tullis, T. E., & Weeks, J. D. (1988). Roughness and wear during brittle faulting. *Journal of Geophysical Research*, 93(B12), 15268–15278. <https://doi.org/10.1029/jb093ib12p15268>
- Preuss, S., Herrendörfer, R., Gerya, T., Ampuero, J. P., & van Dinther, Y. (2019). Seismic and aseismic fault growth lead to different fault orientations. *Journal of Geophysical Research: Solid Earth*, 124(8), 8867–8889. <https://doi.org/10.1029/2019JB017324>
- Radiguet, M., Cotton, F., Manighetti, I., Campillo, M., & Douglas, J. (2009). Dependency of near-field ground motions on the structural maturity of the ruptured faults. *Bulletin of the Seismological Society of America*, 99(4), 2572–2581. <https://doi.org/10.1785/0120080340>
- Sagy, A., & Brodsky, E. E. (2009). Geometric and rheological asperities in an exposed fault zone. *Journal of Geophysical Research*, 114(B2), B02301. <https://doi.org/10.1029/2008JB005701>
- Sagy, A., Brodsky, E. E., & Axen, G. J. (2007). Evolution of fault-surface roughness with slip. *Geology*, 35(3), 283–286. <https://doi.org/10.1130/G23235A.1>
- Schlagenhauf, A., Manighetti, I., Malavieille, J., & Dominguez, S. (2008). Incremental growth of normal faults: Insights from a laser-equipped analog experiment. *Earth and Planetary Science Letters*, 273(3–4), 299–311. <https://doi.org/10.1016/j.epsl.2008.06.042>
- Schwartz, D. P., & Sibson, R. H. (1989). Fault segmentation and controls of rupture initiation and termination. USGS Open-File Report (Vol. 89315, p. 445).

- Segall, P., & Pollard, D. D. (1980). Mechanics of discontinuous faults. *Journal of Geophysical Research*, 85(B8), 4337–4350. <https://doi.org/10.1029/JB085iB08p04337>
- Sibson, R. H. (2003). Thickness of the seismic slip zone. *Bulletin of the Seismological Society of America*, 93(3), 1169–1178. <https://doi.org/10.1785/0120020061>
- Stirling, M. W., Wesnousky, S. G., & Shimazaki, K. (1996). Fault trace complexity, cumulative slip, and the shape of the magnitude-frequency distribution for strike-slip faults: A global survey. *Geophysical Journal International*, 124(3), 833–868. <https://doi.org/10.1111/j.1365-246X.1996.tb05641.x>
- Thakur, P., Huang, Y., & Kaneko, Y. (2020). Effects of low-velocity fault damage zones on long-term earthquake behaviors on mature strike-slip faults. *Journal of Geophysical Research: Solid Earth*, 125(8), e2020JB019587. <https://doi.org/10.1029/2020JB019587>
- Wechsler, N., Ben-Zion, Y., & Christofferson, S. (2010). Evolving geometrical heterogeneities of fault trace data. *Geophysical Journal International*, 182(2), 551–567. <https://doi.org/10.1111/j.1365-246X.2010.04645.x>
- Wesnousky, S. G. (1988). Seismological and structural evolution of strike-slip faults. *Nature*, 335(6188), 340–343. <https://doi.org/10.1038/335340a0>